REGULAR ARTICLE

blood advances

Phosphoproteomics and morphology of stored human red blood cells treated by protein tyrosine phosphatases inhibitor

Manon Bardyn,[1] David Crettaz,[1] Benjamin Rappaz,[2] Romain Hamelin,[3] Florence Armand,[3] Jean-Daniel Tissot,[1] Gerardo Turcatti,[2] and Michel Prudent[1,4,5]

[1]Laboratoire de Recherche sur les Produits Sanguins, Transfusion Interrégionale CRS, Epalinges, Switzerland; [2]Biomolecular Screening Facility and [3]Proteomics Core Facility, Ecole Polytechnique Fédérale de Lausanne, Lausanne, Switzerland; [4]Center for Research and Innovation in Clinical Pharmaceutical Sciences, Lausanne University Hospital and University of Lausanne, Lausanne, Switzerland; and [5]Institute of Pharmaceutical Sciences of Western Switzerland, University of Geneva, Geneva, Switzerland

Key Points

- Protein tyrosine phosphorylation is lost during the storage of RBCs for transfusion purposes.
- The use of KIs pointed out that different phosphoproteins alter the stability of membrane proteins and cytoskeleton linkage.

The process of protein phosphorylation is involved in numerous cell functions. In particular, phosphotyrosine (pY) has been reported to play a role in red blood cell (RBC) functions, including the cytoskeleton organization. During their storage before transfusion, RBCs suffer from storage lesions that affect their energy metabolism and morphology. This study investigated the relationship between pY and the storage lesions. To do so, RBCs were treated (in the absence of calcium) with a protein tyrosine phosphatase inhibitor (orthovanadate [OV]) to stimulate phosphorylation and with 3 selective kinase inhibitors (KIs). Erythrocyte membrane proteins were studied by western blot analyses and phosphoproteomics (data are available via ProteomeXchange with identifier PXD039914) and cell morphology by digital holographic microscopy. The increase of pY triggered by OV treatment (inducing a global downregulation of pS and pT) disappeared during the storage. Phosphoproteomic analysis identified 609 phosphoproteins containing 1752 phosphosites, of which 41 pY were upregulated and 2 downregulated by OV. After these phosphorylation processes, the shape of RBCs shifted from discocytes to spherocytes, and the addition of KIs partially inhibited this transition. The KIs modulated either pY or pS and pT via diverse mechanisms related to cell shape, thereby affecting RBC morphology. The capacity of RBCs to maintain their function is central in transfusion medicine, and the presented results contribute to a better understanding of RBC biology.

Introduction

During ex vivo aging, red blood cells (RBCs) suffer from lesions[1-4] that are characterized, among other parameters, by changes in cell morphology and increased cell rigidity.[5,6] Alterations of cell shape and deformability result from different features influenced by vesiculation, osmolarity, and ion transport, as well as membrane proteins/lipids reorganization in active or passive events.[7-9]

The membrane/cytoskeleton interactions (rupture of which is observed in several diseases)[7] regulate the RBC shape change in an adenosine triphosphate (ATP)-dependent manner.[10] To soften its

Submitted 9 February 2023; accepted 24 October 2023; prepublished online on *Blood Advances* First Edition 1 November 2023. https://doi.org/10.1182/bloodadvances.2023009964.

The mass spectrometry proteomics data have been deposited to the ProteomeXchange Consortium via the PRoteomics IDEntifications partner repository with the data set identifier PXD039914.

Additional data are available upon reasonable request from the corresponding author, Michel Prudent (Michel.Prudent@itransfusion.ch).

The full-text version of this article contains a data supplement.

cytoskeleton, RBCs expend energy in the form of ATP, which induces enhanced membrane fluctuations and cell shape change.[11] The nonequilibrium dynamism is due to the dissociation of the cytoskeleton at the spectrin junctions powered by ATP. Once dissociated from the cytoskeleton, the membrane fluctuations are thermally governed.[12] Several groups evoked the hypothesis of protein phosphorylation in the regulation of membrane deformability.[10,11,13-16]

Phosphorylation (eg, band 3) is known to regulate enzymatic activity in RBCs,[17,18] and the phosphorylation of cytoskeleton and membrane proteins has been reported to modulate protein-protein interactions.[15,16] These modifications involve adducin, β-spectrin, protein 4.1, as well as band 3. A few proteomic studies focusing on *Plasmodium falciparum*–infected RBCs and sickle cell disease identified several phosphoproteins.[19-21] They pointed out their roles in signaling and RBC deformability (through the phosphorylation of proteins belonging to the junctional complex).[22] Lately, another one highlighted the role of a set of phosphoproteins involved in deformability experiments.[23] As for transfusion medicine, Rinalducci et al quantified by label-free phosphoproteomics a few membrane phosphoproteins, including β-spectrin, ankyrin-1, α-adducin, dematin, glycophorin A, and glycophorin C, and observed the upregulation of targeted phosphoserines during storage.[24]

Phosphorylation of band 3 has been studied since the 1980s.[25] Low et al detected the presence of 2 kinases in RBCs, $p72^{syk}$ (Syk) and $p56/53^{lyn}$ (Lyn), and demonstrated that Syk was responsible for band 3 phosphorylation under pervanadate treatment.[26] Later, Brunati et al reported the sequential phosphorylation of band 3 by Syk on Tyr8 and Tyr21 and Lyn on Tyr359 and Tyr904 (independent of Syk in the case of chorea-acanthocytosis).[27,28] They also discovered the role of SHP-2 protein tyrosine phosphatase (PTP) in the dephosphorylation of band 3 and Syk-mediated phosphorylation.[29]

Protein phosphorylation could favor morphological changes in response to stress.[15,23,30,31] Ferru et al proposed a phosphorylation-induced oxidation mechanism in which Syk binds to oxidized band 3, phosphorylates it, and causes the weakening of the cytoskeleton and the formation of band 3 clusters. Those aggregates are released in microvesicles in thalassemia and G6PD deficiency.[30,31] Conversely, Minetti et al suggested that band 3 phosphorylation was not a prerequisite in Ca^{2+}/ionophore-induced microvesicles.[32] Under blood banking conditions, in which oxidative processes play a central role,[33-37] microvesicles accumulate during storage. So far, the link to phosphorylation remains unknown.

Several questions remain open regarding all these mechanisms of regulation. Indeed, the phosphorylation of proteins along the storage of RBCs has mainly been explored regarding band 3. Our goal here was to investigate both the Tyr-phosphorylation (pY)–dependent shape change as well as to relate them to the effect of aging under blood banking conditions. For this purpose, RBC morphology was studied by digital holographic microscopy (DHM)[38-40] using inhibitors of PTPs and protein tyrosine kinases. In addition, protein phosphorylation was quantified and characterized by Western blot (WB) and phosphoproteomics. This multidisciplinary approach comprehensively depicts the role of protein phosphorylation on RBC morphology and the impact of storage on this mechanism.

Methods

RBC concentrate (RCC)

Blood collected from healthy donors was prepared in top-bottom bags system (CompoFlow CQ32250, Fresenius Kabi). A total of 450 ± 50 mL of whole blood mixed with 63 mL of CPD (citrate-phosphate-dextrose) anticoagulant was centrifuged, the components were separated, RBC fraction was filtrated to remove residual leucocytes, and 100 mL of SAGM (saline-adenine-glucose-mannitol) additive solution was added for storage. RCCs were kept at 4°C for up to 6 weeks. Six RCCs were used for the phosphoproteomic and WB experiments under orthovanadate (OV) treatment, 6 others to evaluate the effect of kinase inhibitors (KIs), and 3 more for DHM with KIs. The project was accepted by the institutional review board of Transfusion Interrégionale Croix-Rouge suisse (CRS), in compliance with local legislation, and was conducted according to the Declaration of Helsinki.

Treatment of RBCs

Samples were drawn from RCC using sterile needles and syringes through a sampling site. To retrieve RCC supernatant for hemolysis measurement, samples were centrifuged for 10 minutes at 2000*g* and 4°C. RBC pellets were washed 1 to 2 times in 0.9% NaCl and resuspended in HEPA buffer (15 mM Hepes, 1 g/L bovine serum albumin, 130 mM NaCl, 5.4 mM KCl, 0.5 mM $MgCl_2{\cdot}6H_2O$, 10 mM glucose, and pH 7.4). Chemicals were purchased from Sigma-Aldrich (Steinheim, Germany), MSD Merck Sharp & Dohme (Luzern, Switzerland), Laboratorium Dr. G. Bichsel (Interlaken, Switzerland), and MP Biomedicals (Illkirch, France). KIs were from Selleckchem (Houston, TX).

RBCs were treated with 2 mM of phosphatase inhibitor sodium OV (Na_3VO_4, OV)[15] or dH_2O (control) for 1 hour or 4 hours at 37°C either in tubes (under agitation) or in a 96-well plate for microscopy experiments (see below). To test the impact of KIs, RBCs were first treated with 10 μM of KI (Saracatinib, S1006, against Src; PRT062607, S8032, against Syk; bafetinib, S1369, against Lyn; PD153035, S6546, against EGFR; H89, S1582, against protein kinase A [PKA]; Go 6983, S2911, against PKC; and D4476, S7642, and Silmitasertib, S2248, against casein kinase) or dimethyl sulfoxide (DMSO; control) for 1 hour at 37°C before incubation with OV.

Hematological parameters

Hematological data were recorded with an automated hematology analyzer (KX-21N, Sysmex). Microvesicles were quantified by flow cytometry (FACScalibur flow cytometer with CellQuest pro software; BD Biosciences, Franklin Lakes, NJ).[40] Supernatant hemoglobin concentration was determined according to the Harboe method[41] by spectrophotometry (NanoDrop 2000c, Thermo Scientific, Wilmington, DE). Samples were diluted in dH_2O if required (ie, A_{415} above 1.5 arbitrary unit (A.U.)).

Membrane proteins extraction

For WB and phosphoproteomic analyses, RBCs were lysed by incubation in hypotonic buffer (0.1× phosphate-buffered saline) for 1 hour at 4°C on a roller, in the presence of 2 mM OV or dH_2O (control) plus 10 μM KI or 0.1% DMSO (control). Cell lysates were centrifuged at 21 500*g* in 4°C for 75 minutes to isolate membranes. Membranes were washed in 0.1× phosphate-buffered

saline (centrifugation cycles of 30 min) until white pellets were obtained. Aliquots were saved at −80°C.

Phosphoproteomics

Membrane proteins were extracted in 4 volumes of 8 M urea, 2 M thiourea, 0.5% sodium dodecyl sulfate (SDS), and 10 mM dithioerythritol (DTE). Each sample was in-solution digested with Lys-C (1:50 enzyme/protein) and then with trypsin gold (1:50 enzyme/protein). Phosphopeptides were desalted and enriched on titania tips[42] and analyzed by liquid chromatography (Dionex Ultimate 3000 RSLC nanoUPLC system; Thermo Scientific, Rockford, IL) coupled to an Orbitrap Q-Exactive HF (Exploris 480 Mass spectrometer for KIs, Thermo Scientific). Raw data were treated using MaxQuant 1.6.0.16 (1.6.10.43 for KIs)[43] with Andromeda as an internal database search engine.[44] Fragmentation spectra were searched against the human UniProt database (July 2017; 71 567 sequences). A *t* test analysis was performed using Perseus 1.6.0.7,[45] and graphs were generated with homemade programs (R environment).[46] Class 1 phosphosites with intensities in monophosphopeptides (multiplicity = 1), with at least 12 valid values in at least 1 group (OV or Control), were kept for the analysis (3 valid values in at least 1 group for KIs). The significantly differentially quantified phosphosites were defined according to a permutation-based multiple-testing analysis (250 permutations; false discovery rate (FDR) = 0.05; S0 = 1; and S0 = 0.1 for the KIs).

WB analysis against phosphotyrosines

Membrane/cytoskeleton proteins were extracted from pelleted membranes with 4 to 6 volumes of deoxycholate (DC) buffer: 1% DC in 50 mM Tris-HCl, 150 mM NaCl, and pH 8.1.[34] Ten µg of proteins from each sample and 10 µL of BenchMark Pre-Stained Protein Ladder (Invitrogen, ThermoFisher Scientific) were loaded on sodium dodecyl sulfate polyacrylamide gel electrophoresis (SDS-PAGE, Mini-PROTEAN TGX gels, 4%-15%; BIO-RAD). WB were performed on polyvinylidene fluoride (PVDF) membranes against pY-containing proteins (pY PY99 1/6000 from Santa Cruz Biotechnology, Dallas, TX). Washing and incubation with primary and secondary antibodies were done in tris-buffered saline (TBS-T: 1× TBS + 0.05% Tween-20) and Top Block buffer (Sigma-Aldrich, 4% in TBS-T), respectively. Secondary antibody (polyclonal goat antimouse immunoglobulins HRP, Dako) was diluted at 1/6000 or 1/10 000 in Top Block buffer. Bands of interest (from WB and Ponceau red staining) were quantified by densitometry (ImageQuant TL software 7.0; GE Healthcare, Uppsala, Sweden) and expressed as "volume." pY signals were normalized by total protein loading.

Morphology analysis

Quantitative phase images were acquired using a DHM T1000 (Lyncée Tec SA, Lausanne, Switzerland). DHM provides label-free measurements of the optical path difference (OPD), a parameter proportional to the refractive index and thickness of the sample.[38,47] For imaging, RBCs were seeded (80 000 per well) in a 96-well plate coated with 0.1 mg per mL Poly-L-ornithine.[40] To speed up cell sedimentation, the plate was centrifuged at room temperature for 2 minutes at 140*g*. Then, the plate was placed in a Chamlide WP Incubator System (LCI Live Cell Instrument, Seoul, South Korea) set at 37°C with high humidity and 5% CO_2. Four images, obtained at a 20× magnification (Leica 20×/0.40 NA objective; Leica Microsystems GmbH, Wetzlar, Germany), were taken in each well, with 4 wells per condition. First, 4 baseline images were acquired at a 5-minute interval. The RBCs were then treated with 0.1% DMSO (control) or 10 µM KI and incubated for 45 minutes (10 acquisitions, each 5 minutes). Finally, the RBCs were treated with 2 mM OV or dH_2O (control). Timelapse images were recorded every half hour for ~20 hours.

Images were analyzed in 2 different ways. A population analysis was performed by calculating the spatial standard deviation of the OPD (SD-OPD) value.[40] Single-cell phenotypic analysis was also performed using CellProfiler (Broad Institute, www.cellprofiler.org, 2.1.0 rev 0c7fb94)[48] and CellProfiler Analyst (2.0 r11710)[49] to sort RBCs as: "discocytes," "echinocytes," "spherocytes," and "errors." For analysis of timelapse experiments, the area under the curve (AUC) parameter was selected because it integrates information about the behavior of the RBCs during the whole timelapse period.

Data analysis

GraphPad Prism (version 8.4.2 [464], GraphPad Software, LLC, San Diego, CA) was used for data presentation and statistical analyses.

Results

Phosphoproteomics of RBC membrane under OV treatment

A label-free quantitative phosphoproteomic analysis of RBC membrane proteins treated or not with OV was carried out to identify and quantify phosphoproteins. It revealed the presence of 1949 phosphopeptides (1752 Class 1 phosphosites, ie, localization probability > 0.75, and 801 quantified Class 1 monophosphosites) distributed over 609 phosphoproteins (Figure 1A; supplemental Material 2, SM-2; additional data available ProteomeXchange).[50] The proportion of pS, pT, and pY Class 1 monophosphosites is 84.3%, 8.1%, and 7.6%, respectively. Upon OV treatment (PTP inhibition), 41 of 61 pY-sites belonging to 22 different proteins were significantly upregulated (Figure 1B) and 2 downregulated (see list in supplemental Material 3, SM-3). The first 20 upregulated pY-sites belong to proteins mainly involved in the cell structure: band 3 (gene name *SLC4A1*), α- and β-spectrin (*SPTA1* and *SPTB*), α- and β-adducin (*ADD1* and *ADD2*), protein 4.1 (*EPB41*), ankyrin-1 (*ANK1*), dematin (*DMTN*), and tensin-1 (*TNS1*), which is coherent with WB presented in Figure 2A. A network analysis (String-db.org, version 11.5, December 2022; Figure 1C) shows a cluster of these proteins involved in band 3–ankyrin and junctional complexes, in connection to kinase activities with nonspecific protein tyrosine kinase (*YES1*, *LCK*, *SRC,* or *FYN*, shared identified peptide) and Lyn kinase (*LYN*), as well as other proteins including flotillin-2 (*FLOT2*), aquaporin-1 (*AQP1*), receptor protein tyrosine kinase (*EPHB4*) and phosphatidylinositol 3,4,5-trisphosphate 5-phosphatase 1 (*INPP5D*).

In addition to pY modifications triggered by OV, pS and pT were also significantly regulated (see black dots; Figure 1B). Altogether, 60 and 123 phosphosites were significantly upregulated and downregulated, respectively, which indicated a global downregulation when pY were upregulated.

Response to OV according to RCC aging

Accumulation of pY under OV treatment was confirmed by WB analyses. Figure 2A shows the pY signal after 1 or 4 hours of OV treatment in RBCs stored for 1, 21, or 42 days. The pY signals

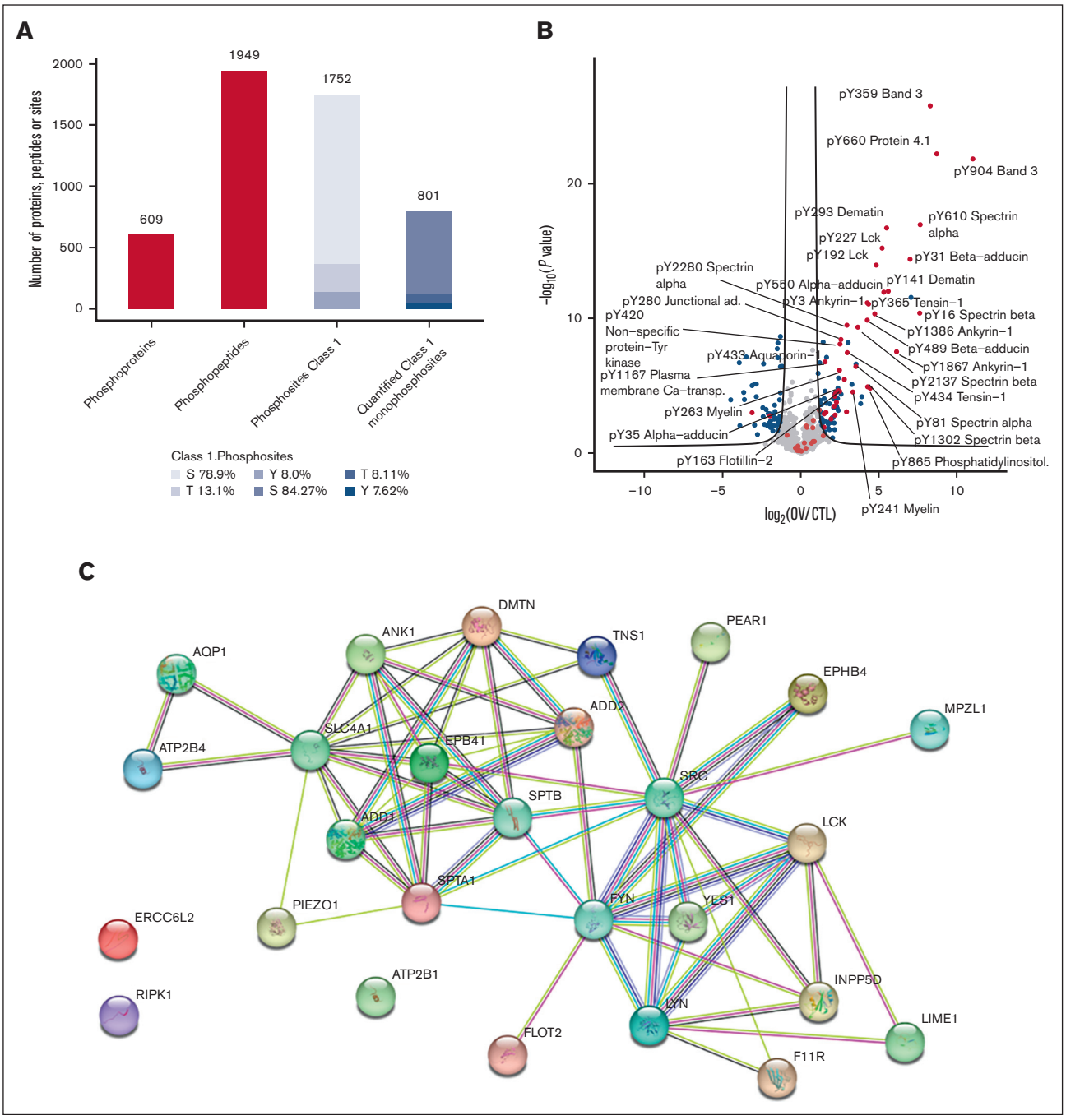

Figure 1. Phosphoproteomics of OV-treated RBC membrane proteins. RBCs from RCCs at day 2 of storage (n = 6) were analyzed. (A) Phosphoproteome-depth: number of identified phosphoproteins, phosphopeptides, phosphosites, and class 1 phosphosites. The number of phosphosites (class 1 or quantified class 1) are presented in different colors of blue. (B) Comparison of phosphosites after 1 hour of OV treatment vs without any treatment. Volcano plot showing *t* test *P* values (log10) vs phosphosite fold changes (log2). Blue points correspond to class 1 phosphosites (multiplicity 1) differentially quantified, and unchanged phosphosites are in gray. Significant pY are highlighted in red and nonsignificant in light red. The black curves correspond to a FDR < 0.05 and a S0 = 1. (C) Protein-protein interactions of upregulated and downregulated (the 2 on the bottom left) phosphoproteins.

were observed on specific protein bands, corresponding to (top to bottom) α-spectrin, β-spectrin, ankyrin-1, α-adducin, β-adducin, band 3, and protein 4.1. Two bands around 70 kDa could correspond to Lyn and Syk kinases. During RBC storage, the effect of OV decreased progressively (Figure 2A, right). At day 42, only a weak signal was detected.

OV treatment induced the release of microvesicles and hemolysis (Figure 2B). This effect is visible after 4 hours of incubation but not after 1 hour. Consistent with the phosphorylation levels, RBCs stored for 1 day released a higher number of microvesicles and hemolyzed more (not significant) than RBCs stored for 21 or 42 days.

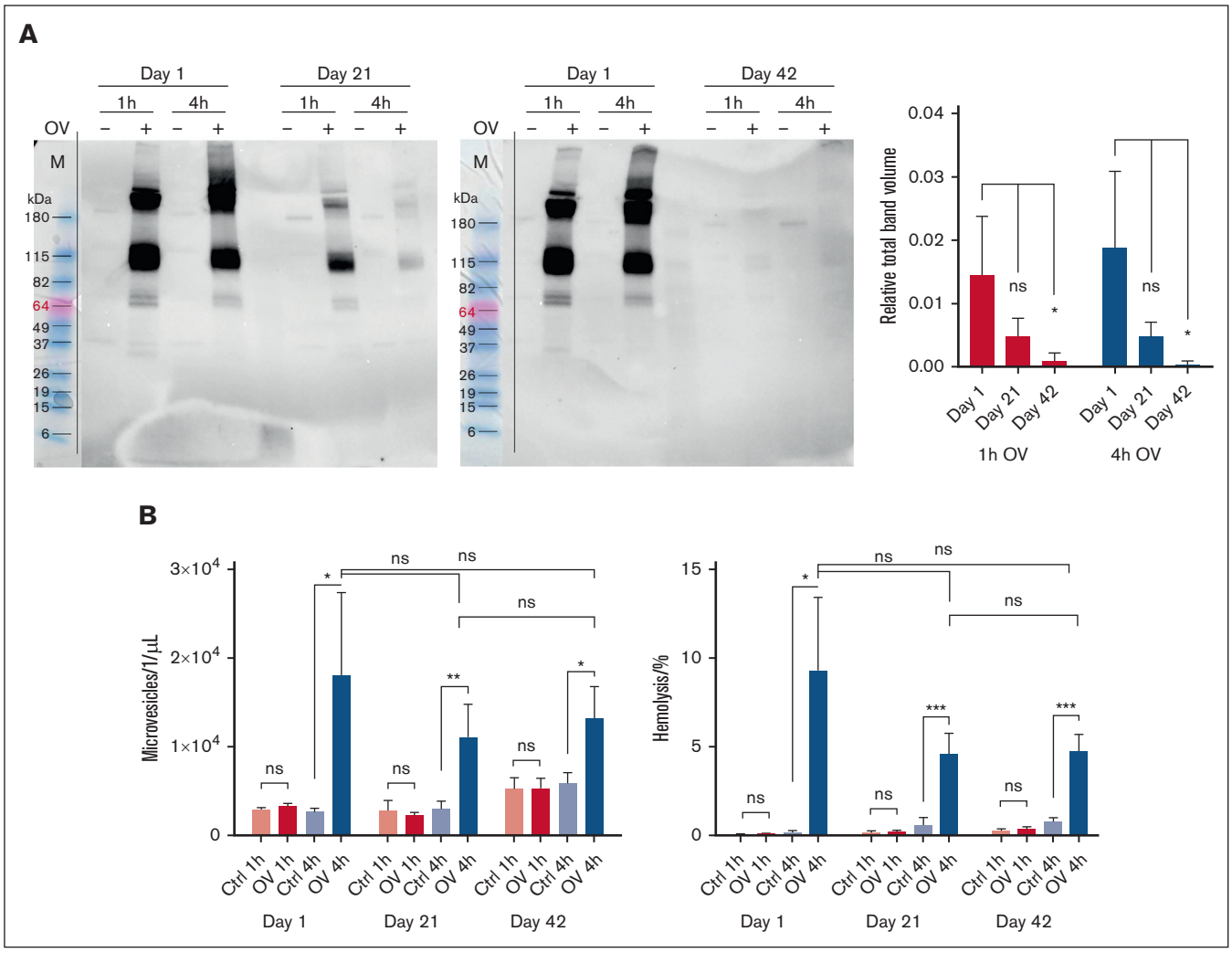

Figure 2. Membrane proteins tyrosine phosphorylation, microvesiculation, and hemolysis in OV-treated RBCs. RCCs (n = 6) stored for 1, 21, and 42 days were analyzed, mean values ± SD are displayed on the graphs. *P* values, Tukey multiple comparison test: ns $P > .05$; *$P \leq .05$; **$P \leq .01$; ***$P \leq .001$. (A) WB analysis against pY-containing membrane proteins of RBCs treated 2 mM OV for 1 or 4 hours. (A, left) Representative image of WB experiment (RCC 2), note that the molecular weight marker bands (M) were superimposed on the chemiluminescence pictures; (A, right) Total relative pY signal (ie, the sum of pY-positive bands normalized by total protein loading [ponceau red]). (B, left) Concentration of microvesicles released; and (B, right) level of hemolysis after 1 or 4 hours of treatment.

Impact on cell morphology

In the control group (0.1% DMSO), the SD-OPD signal (linearly correlated to the percentage of spherocytes)[40] slightly increased throughout the 20-hour timelapse, whereas it increased rapidly until reaching a plateau for OV-treated RBCs (Figure 3A). The AUC value, corresponding to integration of SD-OPD over time, was equivalent in both storage age of RCCs, with an upward trend at storage day 40.

Analysis of single-cell phenotype by automated analysis of phase images (Figure 3C) confirmed that the increase of SD-OPD signal was due to the rapid formation of echinocytes (intermediate shape) and spherocytes, concomitant to a drop-down of discocytes (Figure 3B). Morphological changes after OV treatment appeared sooner in older RCCs that were also more sensitive to the experimental conditions, even in the control samples.

Despite a limited number of replicates, the data were consistent with the literature and preliminary data.[15] It has to be noticed that the same phenomena were present with Ca^{2+}-containing HEPA buffer. OV treatment transformed RBCs into spherocytes, and the phosphorylation level in membranes also decreased during storage (supplemental Figures 1 and 2 in SM-1, respectively).[51]

Inhibition of specific kinases

Based on the top-overexpressed phosphoproteins and the literature, the effect of 8 KIs was investigated on the morphology of stored RBCs using a DHM-based screening. Different variations of the SD-OPD were reported during the incubation in the presence of OV+KIs compared with that of OV only and control (SM-1, supplemental Figure 4). Only 3 appeared to decrease SD-OPD values and therefore counteracting the effect of OV. The advanced analyses are presented in Figure 4.

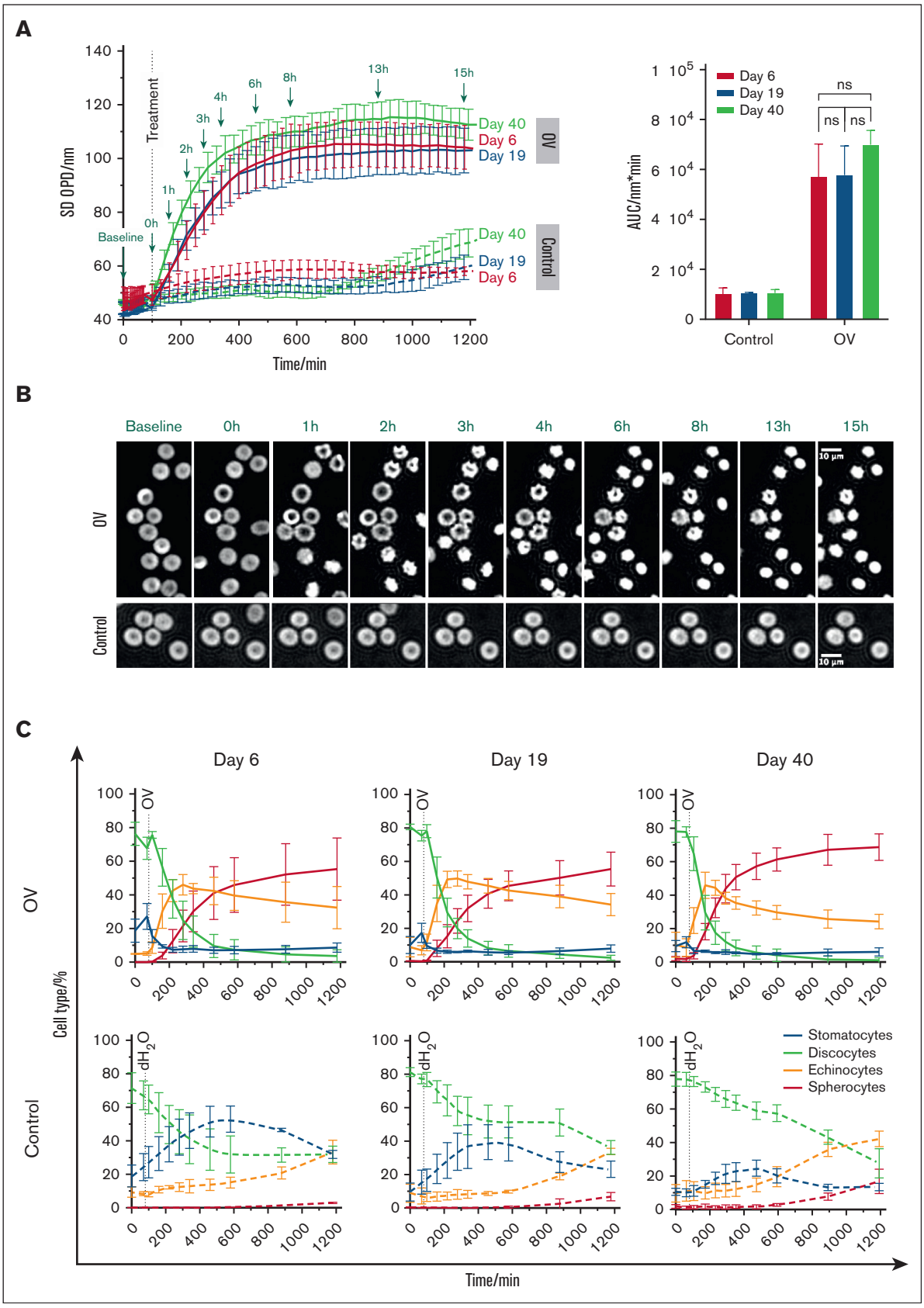
A
SD OPD/nm
Treatment
Baseline
0h
1h
2h
3h
4h
6h
8h
13h
15h
Day 40
Day 6
Day 19
OV
Control
Time/min
AUC/nm*min
Day 6
Day 19
Day 40
ns
Control
OV
B
Baseline
0h
1h
2h
3h
4h
6h
8h
13h
15h
OV
Control
10 µm
C
Day 6
Day 19
Day 40
OV
Control
Cell type/%
dH2O
Stomatocytes
Discocytes
Echinocytes
Spherocytes
Time/min

Figure 3.

The incubation with PRT062607 and bafetinib before the OV treatment drastically abolished the pY process (Figure 4A). However, it was not the case with H89, in which only a weak effect on band 3 was observed. The level of pY on bands corresponding to α-adducin and spectrins was slightly affected.

Phosphoproteomics of KI- and OV-treated RBCs confirmed the differences at the protein level (SM-4). Expressions of phosphosites show shifts in favor of OV, meaning both KIs inhibited the effect of OV treatment (Figure 5). Notably, not only pY sites were significantly downregulated (red dots) when treated with KIs compared with OV, but also pS and pT (blue and gray dots) (SM-5 to 7). As expected, PRT062607 and bafetinib behaved the same, with 12 phosphosites in common, of which 9 were pY. As for H89, pY were not significantly downregulated, and the main modulations concerned pS and pT. Of note, pT378 on protein 4.1 was the only site commonly regulated site to both KIs.

When examining cell morphology, the effects of KIs can be seen through the AUC calculated from the integration of SD-OPD over time (Figure 4B). The presence of KIs on their own increased the AUC value because they favored the stomatocyte phenotype, as shown by image-analysis (Figure 4C). On day 6 of storage, the addition of KIs counterbalanced the effect of OV with a baseline level (Figure 4B). Nonetheless, the inhibitory effect of KIs was less pronounced with increasing storage time (SM-1, supplemental Figure 5). The OV + KIs conditions favored the presence of echinocytes compared with OV only (Figure 4C) and decreased the proportion of spherocytes, suggesting that the KIs delayed the transition from one phenotype to the other.

In summary, the 3 KIs enabled relative cell shape recovery after stimulation of pY, but only bafetinib and PRT062607 entirely abolished the pY phosphorylation, and H89 affected pS and pT.

Discussion

Effect of OV on the RBC phosphoproteome

Two-thousand proteins are known in mature RBCs.[52,53] In their study on RBC deformability, Moura et al detected 63 and 226 phosphoproteins in mature RBCs and reticulocytes, respectively.[23] Phosphoproteomics on sickle cells identified 155 phosphoproteins and 527 phosphosites,[19] and in the case of infected RBCs by *P falciparum*, 1083 phosphosites were detected on 553 proteins.[21] Our data are consistent with these previous sets of data. The higher number of phosphosites in this study is most likely related to the use of a phosphatase inhibitor that exacerbated pY formation.

Several phosphoproteins were remarkably upregulated upon OV treatment, of which a few have already been studied.[26,29] Band 3, α- and β-spectrin, α- and β-adducin, protein 4.1, ankyrin-1, dematin, tensin-1, aquaporin-1, and plasma membrane calcium–transporting ATPase 4 are present within a shared cluster. Indeed, these proteins are part of the well-known band 3–ankyrin and junctional complexes.[54] In addition, Fyn and Lyn were identified. The latter is known to participate in the sequential phosphorylation of band 3 in which Lyn phosphorylates Tyr359 and Tyr904, in a second phase 2[27]; both pY modifications were reported here. Consistently, no phosphorylation on band 3 Tyr8 and Tyr21was detected, which could be explained by direct phosphorylation on Tyr359 and 904.[28] In addition, deletions or modifications (ie, methylation) near tyrosine residues such as aspartate and glutamate in the N-terminal part[55] might affect the detection of phosphosites. Alteration of band 3 is associated with storage lesions and changes RBC properties.[56] As for Fyn, this enzyme is known to phosphorylate spectrins and β-adducin.

Regarding pS and pT, 12 phosphosites are known to be upregulated during RBC storage.[24] Over these phosphosites, 6 were detected in this study (only 2 presenting significant variations). pS122 in glycophorin C was increased in both studies, whereas pS152 in dematin was downregulated here.

Effect of OV on morphology

Concomitant to the OV-induced phosphorylation, a transition from discocytes to spherocytes was observed (Figure 3). The phosphorylation of membrane proteins, particularly band 3 complexes, probably induced a rupture in the cytoskeleton-integral membrane proteins link, initiating shape change. In addition, the binding to protein 4.1 could be inhibited by the phosphorylation on band 3 Y359.[54] Moreover, the Y660 phosphorylation on protein 4.1 is known to disturb the spectrin/actin/4.1 complex.[57] These modifications trigger the formation of spherocytes, similar to spherocytosis with a rupture of the vertical link. The phenotype observed here is similar to previously reported OV-treated RBCs.[15,58] In both studies, the authors showed the formation of echinocytes after 20 or 60 minutes of incubation. In these data, ~30% of echinocytes were detected after 1 hour of treatment. At the end of the incubation period (~20 hours), RBCs were mostly spherocytes. The formation of the spicules could be due to band 3 phosphorylation and clustering, as described by Turrini at al.[15,30,31]

The morphological analyses of OV-treated RBCs showed that the addition of KIs resulted in the enrichment of echinocytes (Figure 4C). The final stage of cell transformation was not reached. It might be explained by the downregulation of phosphorylation on proteins, involved in cell structure, that preserve the link between integral membrane complexes and the cytoskeleton. Therefore, in this timelapse, the formation of spherocytes is partly inhibited.

The 3 KIs had a similar impact on the morphology, even though they caused varying phosphorylation levels. The 2 targeting band 3 (PRT062607 and bafetinib) abolished the pY signals on all proteins, including band 3, protein 4.1, ankyrin-1, and spectrins. In this situation, the similar effect on morphology may be attributed to shared pathways. Bafetinib targets Lyn, which is directly involved in Y359 and Y904 phosphorylations. As for PRT062607, its lower inhibition activity on Lyn could be enough to stop band 3 phosphorylation. In addition, and despite the absence of Syk-induced phosphorylation of band 3 in our proteomic data set, phosphorylation on Syk kinase (pY296) was downregulated (detected but not

Figure 3. Timelapse analysis by DHM of the morphological changes triggered by 2 mM OV treatment. RBCs from RCCs (n = 3) stored for 6, 19, and 40 days were imaged at 20× original magnification, mean values ± SD are displayed. *P* values, Tukey multiple comparison test: ns $P > .05$. (A) Population analysis: (A, left) evolution of SD-OPD signal for 3 RCCs over a 15-hour timelapse analysis; (A, right) AUC obtained by integration of the SD-OPD over time. (B) Phase images illustrating the changes of RBC phenotype. (C) Single-cell analysis with CellProfiler and CellProfiler Analyst. RBCs were classified as "Stomatocytes," "Discocytes," "Echinocytes," or "Spherocytes."

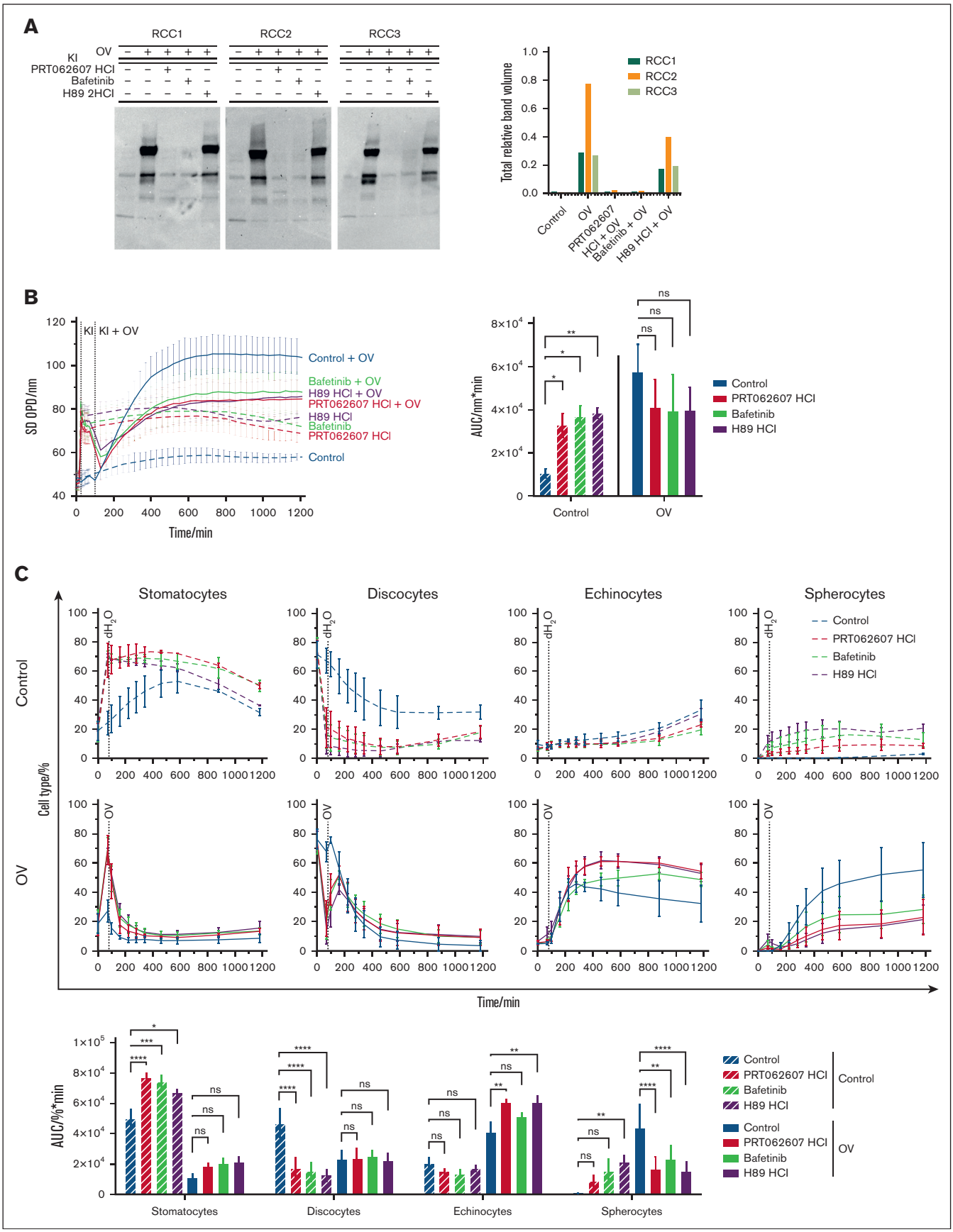
A
RCC1
RCC2
RCC3
KI
OV
PRT062607 HCl
Bafetinib
H89 2HCl
Total relative band volume
RCC1
RCC2
RCC3
Control
OV
PRT062607 HCl + OV
Bafetinib + OV
H89 HCl + OV
B
KI
KI + OV
SD OPD/nm
Time/min
Control + OV
Bafetinib + OV
H89 HCl + OV
PRT062607 HCl + OV
H89 HCl
Bafetinib
PRT062607 HCl
Control
AUC/nm*min
Control
PRT062607 HCl
Bafetinib
H89 HCl
C
Stomatocytes
Discocytes
Echinocytes
Spherocytes
Control
OV
Cell type/%
dH2O
Time/min
AUC/%*min
Control
PRT062607 HCl
Bafetinib
H89 HCl
Control
OV

Figure 4.

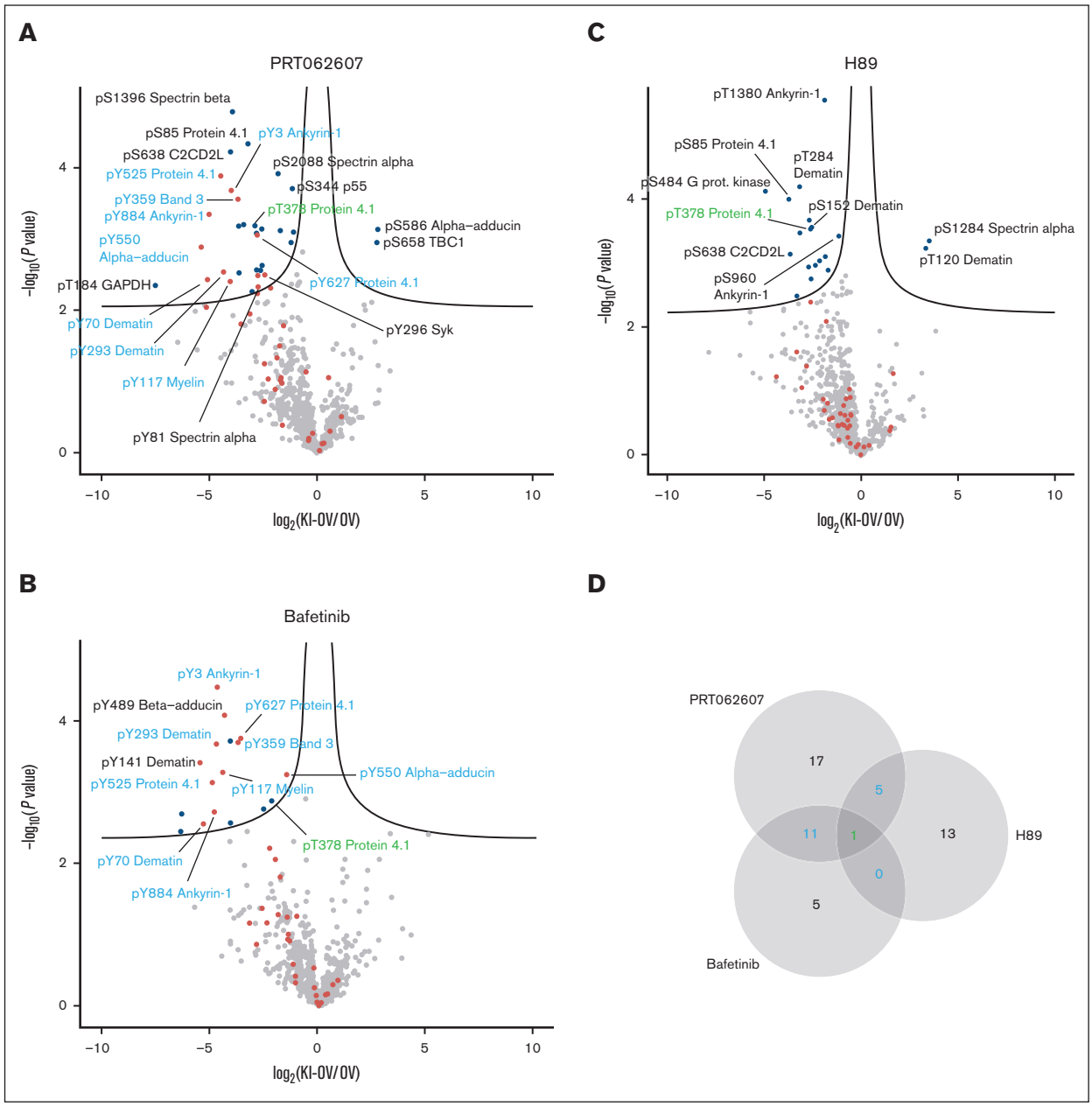

Figure 5. Regulation of the membrane phosphoproteome of OV-treated RBCs with specific KIs. Comparison of phosphosites expression after treatment of RBCs taken in RCCs (3-day-old; n = 6) with KIs ([A] PRT062607, [B] bafetinib, [C] H89) and OV vs an OV treatment only. Volcano plot showing *t* test *P* values (log10) vs phosphosite fold changes (log2). Blue points correspond to class 1 phosphosites (multiplicity 1) differentially quantified and unchanged phosphosites are in gray. Significant pY are highlighted in red and nonsignificant in light red, common pY are highlighted in blue, and the common phosphosite in green. The black curves correspond to an FDR <0.05 and an S0 = 0.1. (D) Venn diagram between the 3 KIs.

Figure 4. Effect of the inhibition of specific kinases on membrane proteins tyrosine phosphorylation and morphology of OV-treated RBCs. RBCs from RCCs (n = 3) were analyzed on day 6. Mean values ± SD are displayed. (A) WB analysis against pY-containing membrane proteins of RBCs treated with 2 mM OV and 10 μM KI. (A, left) Images of the blots; (A, right) total relative pY signal (ie, sum of pY-positive bands normalized by total protein loading [ponceau red]). (B) Morphology analysis by DHM. AUC was obtained by integration of the SD-OPD over time. *P* values, Dunnett multiple comparison test: ns $P > .05$; *$P \leq .05$; **$P \leq .01$. (C) Single-cell analysis with CellProfiler and CellProfiler Analyst. RBCs were classified as "Stomatocytes," "Discocytes," "Echinocytes," or "Spherocytes." (C, top) Evolution over time per cell type; (C, bottom) integration over time. *P* values, Šidák multiple comparison test: ns $P > .05$; *$P \leq .05$; **$P \leq .01$; ***$P \leq .001$, ****$P \leq .0001$.

significantly in the case of bafetinib) and might also inhibit band 3 phosphorylation. The total decrease in pY was also observed on other proteins involved in band 3 complexes, such as protein 4.1. Indeed, the pY660 (detected as pY627 from a truncated form in the KI experiments) was downregulated by both bafetinib and PRT062607. On the contrary, H89 targets PKA involved in adducins and proteins 4.1 and 4.2 phosphorylations but not on Tyr residues, which explains the weak impact on WB.[59] The regulation of other phosphosites (as shown by the phosphoproteomic data, Figure 5C) might significantly impact cell morphology. Although protein 4.1 is expected to be phosphorylated on Y660 by epidermal growth factor receptor (EGFR), it has been reported that PKA can interact with EGFR. Y660 was not affected by H89, but 2 other phosphosites were downregulated by H89 (pS85 and pT378). Therefore, the KI H89 could also counteract the OV-induced phosphorylation of protein 4.1. Suppressing protein 4.1 phosphorylation could protect against the dissociation of spectrin/actin/4.1 complexes. Therefore, it can be speculated that the modifications of PKA-dependent proteins (such as the protein 4.1 and ankyrin-1) have an equivalent impact on morphology but through pS and pT phosphorylations. Additional experiments will be required to investigate such mechanisms.

Effect of storage

The capacity of RBCs to phosphorylate proteins decreases with storage time. A rejuvenation process (that stimulates ATP production)[60-62] restores the ability of protein phosphorylation (supplemental Figure 3 in SM-1).[51] It demonstrates that the enzymes are still functional and that the decrease in phosphorylation is a metabolic issue. Indeed, during storage, RBCs exhibit energy metabolism shifts in which ATP is produced during the first week and then decreases constantly.[4,63,64]

OV is known to induce protein phosphorylation and the formation of spherocytes.[15,58] Nevertheless, the morphology of long-stored RBCs was impacted by the OV treatment (Figure 3A), although no phosphorylation of proteins was detected (Figure 2A). In that case, the effect of OV could be related to (1) the impact of incubation conditions on weakened RBCs[65] or (2) side effects because OV can also inhibit different enzymes.[66,67] OV is a Ca^{2+} pump inhibitor that alters cell morphology in addition to phosphorylation events. Although these experiments were carried out without extracellular Ca^{2+}, it cannot be excluded that changes in intracellular Ca^{2+} induce shape modification, especially in older RCCs.[68] Therefore, the impact on morphology is probably due to pY on short-term stored RBCs (because of phosphorylation capacity, Figure 2A) and ion issues in long-term stored RBCs (absence of phosphorylation capacity). The same effects on morphology and phosphorylation in function of storage time were observed in Ca^{2+}-containing HEPA buffer (SM-1).[51]

As mentioned in the "Introduction," the release of microvesicles[40,69] results from different mechanisms such as phosphorylation, Ca^{2+} entry, and oxidative stress during storage. According to these data and the decrease of phosphorylation capacity proportionally to storage time, the microvesiculation process is probably independent of phosphorylation events in stored RBCs. This effect is consistent with the negative correlation between ATP concentration and microvesiculation[70] as well as the band 3 phosphorylation-independent vesiculation process reported by Minetti et al.[32] However, their microvesicles were Ca^{2+} induced, which is known to recruit specific proteins and have a different composition than storage microvesicles.[71]

The loss of protein phosphorylation ability might be an issue in the transfusion of long-stored RCCs.[3,72] Indeed, it was recently shown on RBCs, especially on reticulocytes, that inhibiting band 3 phosphorylation (using bafetinib and without chemical stimulation) decreases the cell velocity in a microfluidic system.[23] Therefore, problems in pY may render RBC less efficient in crossing capillaries and oxygenating tissues, and in the worst case, it may trigger phagocytosis and RBC clearance.[73,74] Even though this ATP-dependent mechanism was restored in vitro and will be restored in vivo a few hours after transfusion, it is essential to maintain a high phosphorylation capacity to ensure transfusion efficiency. This capacity could be conserved by boosting metabolism (particularly the lower part of glycolysis and the pentose phosphate pathway, because RBCs are devoid of mitochondria).[75]

The data presented here focused on phosphorylation events of RBC membrane proteins and their relation to cell morphology. The membrane phosphoproteomics highlighted many phosphoproteins and phosphosites directly involved in cell morphology. Using KIs pointed out the central role of band 3 and other membrane proteins, such as protein 4.1, in the stability of integral membrane proteins and cytoskeleton linkage. The impact of phosphorylation (even exacerbated here) is central in transfusion medicine, because it is associated with RBC aging in blood bags and, when dysregulated, is known to be involved in many diseases. Metabolic pathways and kinase activity must be investigated further to decipher the reactions controlling these phosphorylation events. The reported results and the further studies they suggest will contribute to enriching our knowledge in hematology.

Acknowledgments

The authors thank E. Längst for complementary experiments on rejuvenation and the Foundation SRTS-VD for the financial support.

Authorship

Contribution: M.P. and M.B. designed the experiments and wrote the manuscript; M.B. and D.C. prepared samples and carried out experiments; R.H. and F.A. performed phosphoproteomics and bioinformatics analyses, respectively, and they analyzed data and contributed to the writing of the manuscript; J.-D.T., B.R., and G.T. reviewed the data and manuscript; and all the authors read and approved the final manuscript.

Conflict-of-interest disclosure: B.R. is an employee of Lyncée Tec SA, which commercializes digital holographic microscopy. The remaining authors declare no competing financial interests.

Current affiliation: M.B., Biomolecular Screening Facility, Ecole Polytechnique Fédérale de Lausanne, Lausanne, Switzerland.

ORCID profiles: M.B., 0000-0003-0051-8232; B.R., 0000-0002-8744-600X; J.-D.T., 0000-0003-2493-8469; G.T., 0000-0003-0139-223X; M.P., 0000-0001-9470-0179.

Correspondence: Michel Prudent, Transfusion Interrégionale CRS, Biopôle Secteur Croisettes - Bâtiment Metio, Rte de la Corniche 2, 1066 Epalinges, Switzerland; email: Michel.Prudent@itransfusion.ch.

References

1. Hess JR, Greenwalt TG. Storage of red blood cells: new approaches. *Transfus Med Rev*. 2002;16(4):283-295.
2. Flatt JF, Bawazir WM, Bruce LJ. The involvement of cation leaks in the storage lesion of red blood cells. *Front Physiol*. 2014;5(214):214.
3. Prudent M, Tissot JD, Lion N. In vitro assays and clinical trials in red blood cell aging: lost in translation. *Transfus Apher Sci*. 2015;52(3):270-276.
4. Yoshida T, Prudent M, D'Alessandro A. Red blood cell storage lesion: causes and potential clinical consequences. *Blood Transfus*. 2019;17(1):27-52.
5. Sparrow RL, Sran A, Healey G, Veale MF, Norris PJ. In vitro measures of membrane changes reveal differences between red blood cells stored in saline-adenine-glucose-mannitol and AS-1 additive solutions: a paired study. *Transfusion*. 2014;54(3):560-568.
6. Moon I, Yi F, Lee YH, Javidi B, Boss D, Marquet P. Automated quantitative analysis of 3D morphology and mean corpuscular hemoglobin in human red blood cells stored in different periods. *Opt Express*. 2013;21(25):30947-30957.
7. Mohandas N, Gallagher PG. Red cell membrane: past, present, and future. *Blood*. 2008;112(10):3939-3948.
8. Lang F, Busch GL, Ritter M, et al. Functional significance of cell volume regulatory mechanisms. *Physiol Rev*. 1998;78(1):247-306.
9. Huisjes R, Bogdanova A, van Solinge WW, Schiffelers RM, Kaestner L, van Wijk R. Squeezing for life – properties of red blood cell deformability. *Front Physiol*. 2018;9:656.
10. Gov NS, Safran SA. Red blood cell membrane fluctuations and shape controlled by ATP-induced cytoskeletal defects. *Biophys J*. 2005;88(3):1859-1874.
11. Park YK, Best CA, Auth T, et al. Metabolic remodeling of the human red blood cell membrane. *Proc Natl Acad Sci U S A*. 2010;107(4):1289-1294.
12. Boss D, Hoffmann A, Rappaz B, et al. Spatially-resolved eigenmode decomposition of red blood cells membrane fluctuations questions the role of ATP in flickering. *PLoS One*. 2012;7(8):e40667.
13. Boivin P. Role of the phosphorylation of red blood-cell membrane-proteins. *Biochem J*. 1988;256(3):689-695.
14. Levin S, Korenstein R. Membrane fluctuations in erythrocytes are linked to MgATP-dependent dynamic assembly of the membrane skeleton. *Biophys J*. 1991;60(3):733-737.
15. Ferru E, Giger K, Pantaleo A, et al. Regulation of membrane-cytoskeletal interactions by tyrosine phosphorylation of erythrocyte band 3. *Blood*. 2011;117(22):5998-6006.
16. Gauthier E, Guo XH, Mohandas N, An XL. Phosphorylation-dependent perturbations of the 4.1R-associated multiprotein complex of the erythrocyte membrane. *Biochemistry*. 2011;50(21):4561-4567.
17. Harrison ML, Rathinavelu P, Arese P, Geahlen RL, Low PS. Role of band-3 tyrosine phosphorylation in the regulation of erythrocyte glycolysis. *J Biol Chem*. 1991;266(7):4106-4111.
18. Lewis IA, Campanella ME, Markley JL, Low PS. Role of band 3 in regulating metabolic flux of red blood cells. *Proc Natl Acad Sci U S A*. 2009;106(44):18515-18520.
19. Soderblom EJ, Thompson JW, Schwartz EA, et al. Proteomic analysis of ERK1/2-mediated human sickle red blood cell membrane protein phosphorylation. *Clin Proteomics*. 2013;10(1):1.
20. Siciliano A, Turrini F, Bertoldi M, et al. Deoxygenation affects tyrosine phosphoproteome of red cell membrane from patients with sickle cell disease. *Blood Cells Mol Dis*. 2010;44(4):233-242.
21. Wang J, Jiang N, Sang X, et al. Protein modification characteristics of the malaria parasite Plasmodium falciparum and the infected erythrocytes. *Mol Cell Proteomics*. 2021;20:100001.
22. Burton NM, Bruce LJ. Modelling the structure of the red cell membrane. *Biochem Cell Biol*. 2011;89(2):200-215.
23. Moura PL, Lizarralde Iragorri MA, Français O, et al. Reticulocyte and red blood cell deformation triggers specific phosphorylation events. *Blood Adv*. 2019;3(17):2653-2663.
24. Rinalducci S, Longo V, Ceci LR, Zolla L. Targeted quantitative phosphoproteomic analysis of erythrocyte membranes during blood bank storage. *J Mass Spectrom*. 2015;50(2):326-335.
25. Dekowski SA, Rybicki A, Drickamer K. A tyrosine kinase associated with the red-cell membrane phosphorylates band-3. *J Biol Chem*. 1983;258(5):2750-2753.
26. Harrison ML, Isaacson CC, Burg DL, Geahlen RL, Low PS. Phosphorylation of human erythrocyte band-3 by endogenous p72(syk). *J Biol Chem*. 1994;269(2):955-959.
27. Brunati AM, Bordin L, Clari G, et al. Sequential phosphorylation of protein band 3 by Syk and Lyn tyrosine kinases in intact human erythrocytes: identification of primary and secondary phosphorylation sites. *Blood*. 2000;96(4):1550-1557.
28. De Franceschi L, Tomelleri C, Matte A, et al. Erythrocyte membrane changes of chorea-acanthocytosis are the result of altered Lyn kinase activity. *Blood*. 2011;118(20):5652-5663.
29. Bordin L, Ion-Popa F, Brunati AM, Clari G, Low PS. Effector-induced Syk-mediated phosphorylation in human erythrocytes. *Biochim Biophys Acta*. 2005;1745(1):20-28.
30. Ferru E, Pantaleo A, Carta F, et al. Thalassemic erythrocytes release microparticles loaded with hemichromes by redox activation of p72Syk kinase. *Haematologica*. 2014;99(3):570-578.

31. Pantaleo A, Ferru E, Carta F, et al. Irreversible AE1 tyrosine phosphorylation leads to membrane vesiculation in G6PD deficient red cells. *PLoS One*. 2011;6(1):e15847.
32. Minetti G, Piccinini G, Balduini C, Seppi C, Brovelli A. Tyrosine phosphorylation of band 3 protein in Ca2+/A23187-treated human erythrocytes. *Biochem J*. 1996;320(pt 2):445-450.
33. Antonelou MH, Kriebardis AG, Stamoulis KE, Economou-Petersen E, Margaritis LH, Papassideri IS. Red blood cell aging markers during storage in citrate-phosphate-dextrose-saline-adenine-glucose-mannitol. *Transfusion*. 2010;50(2):376-389.
34. Delobel J, Prudent M, Rubin O, Crettaz D, Tissot J-D, Lion N. Subcellular fractionation of stored red blood cells reveals a compartment-based protein carbonylation evolution. *J Proteomics*. 2012;76 Spec No.:181-193.
35. Reisz JA, Wither MJ, Dzieciatkowska M, et al. Oxidative modifications of glyceraldehyde 3-phosphate dehydrogenase regulate metabolic reprogramming of stored red blood cells. *Blood*. 2016;128(12):e32-42.
36. Bardyn M, Tissot JD, Prudent M. Oxidative stress and antioxidant defenses during blood processing and storage of erythrocyte concentrates. *Transfus Clin Biol*. 2018;25(1):96-100.
37. Yasemi M, Prudent M, Jolicoeur M. A dynamic constraint-based modelling (DCBM) approach with alternative metabolic objective functions predicts the impact of oxidative stress on stored red blood cells (RBCs). *IFAC-PapersOnLine*. 2022;55(20):385-390.
38. Rappaz B, Barbul A, Emery Y, et al. Comparative study of human erythrocytes by digital holographic microscopy, confocal microscopy, and impedance volume analyzer. *Cytometry A*. 2008;73(10):895-903.
39. Bardyn M, Allard J, Crettaz D, et al. Image- and fluorescence-based test shows oxidant-dependent damages in red blood cells and enables screening of potential protective molecules. *Int J Mol Sci*. 2021;22(8):4293.
40. Bardyn M, Rappaz B, Jaferzadeh K, et al. Red blood cells ageing markers: a multi-parametric analysis. *Blood Transfus*. 2017;15(3):239-248.
41. Han V, Serrano K, Devine DV. A comparative study of common techniques used to measure haemolysis in stored red cell concentrates. *Vox Sang*. 2010;98(2):116-123.
42. Cox J, Matic I, Hilger M, et al. A practical guide to the MaxQuant computational platform for SILAC-based quantitative proteomics. *Nat Protoc*. 2009;4(5):698-705.
43. Matz A, Halamoda-Kenzaoui B, Hamelin R, et al. Identification of new Presenilin-1 phosphosites: implication for gamma-secretase activity and A beta production. *J Neurochem*. 2015;133(3):409-421.
44. Cox J, Mann M. MaxQuant enables high peptide identification rates, individualized p.p.b.-range mass accuracies and proteome-wide protein quantification. *Nat Biotechnol*. 2008;26(12):1367-1372.
45. Tyanova S, Temu T, Sinitcyn P, et al. The Perseus computational platform for comprehensive analysis of (prote)omics data. *Nat Methods*. 2016;13(9):731-740.
46. Team RC. R: A Language and Environment for Statistical Computing. R Foundation for Statistical Computing; 2013.
47. Marquet P, Rappaz B, Magistretti PJ, et al. Digital holographic microscopy: a noninvasive contrast imaging technique allowing quantitative visualization of living cells with subwavelength axial accuracy. *Opt Lett*. 2005;30(5):468-470.
48. Carpenter AE, Jones TR, Lamprecht MR, et al. CellProfiler: image analysis software for identifying and quantifying cell phenotypes. *Genome Biol*. 2006;7(10):R100.
49. Jones TR, Kang IH, Wheeler DB, et al. CellProfiler Analyst: data exploration and analysis software for complex image-based screens. *BMC Bioinformatics*. 2008;9:482.
50. Perez-Riverol Y, Bai J, Bandla C, et al. The PRIDE database resources in 2022: a hub for mass spectrometry-based proteomics evidences. *Nucleic Acids Res*. 2022;50(D1):D543-D552.
51. Prudent M, Rappaz B, Hamelin R, et al. Loss of protein Tyr-phosphorylation during in vitro storage of human erythrocytes: impact on RBC morphology. *Transfusion*. 2014;54:49A.
52. Gautier EF, Leduc M, Cochet S, et al. Absolute proteome quantification of highly purified populations of circulating reticulocytes and mature erythrocytes. *Blood Adv*. 2018;2(20):2646-2657.
53. D'Alessandro A, Dzieciatkowska M, Nemkov T, Hansen KC. Red blood cell proteomics update: is there more to discover? *Blood Transfus*. 2017;15(2):182-187.
54. Lux SE. Anatomy of the red cell membrane skeleton: unanswered questions. *Blood*. 2016;127(2):187-199.
55. Reisz JA, Nemkov T, Dzieciatkowska M, et al. Methylation of protein aspartates and deamidated asparagines as a function of blood bank storage and oxidative stress in human red blood cells. *Transfusion*. 2018;58(12):2978-2991.
56. Rogers SC, Ge X, Brummet M, et al. Quantifying dynamic range in red blood cell energetics: evidence of progressive energy failure during storage. *Transfusion*. 2021;61(5):1586-1599.
57. Subrahmanyam G, Bertics PJ, Anderson RA. Phosphorylation of protein 4.1 on tyrosine-418 modulates its function in vitro. *Proc Natl Acad Sci U S A*. 1991;88(12):5222-5226.
58. Bordin L, Clari G, Moro I, Dalla Vecchia F, Moret V. Functional link between phosphorylation state of membrane proteins and morphological changes of human erythrocytes. *Biochem Biophys Res Commun*. 1995;213(1):249-257.

59. Pantaleo A, De Franceschi L, Ferru E, Vono R, Turrini F. Current knowledge about the functional roles of phosphorylative changes of membrane proteins in normal and diseased red cells. *J Proteomics*. 2010;73(3):445-455.
60. Valeri CR, Zaroulis CG. Rejuvenation and freezing of outdated stored human red-cells. *N Engl J Med*. 1972;287(26):1307-1313.
61. Marin M, Roussel C, Dussiot M, et al. Metabolic rejuvenation upgrades circulatory functions of red blood cells stored under blood bank conditions. *Transfusion*. 2021;61(3):903-918.
62. Barshtein G, Arbell D, Livshits L, Gural A. Is it possible to reverse the storage-induced lesion of red blood cells? *Front Physiol*. 2018;9(914):914.
63. Paglia G, D'Alessandro A, Rolfsson O, et al. Biomarkers defining the metabolic age of red blood cells during cold storage. *Blood*. 2016;128(13):E43-E50.
64. Hess JR, D'Alessandro A. Red blood cell metabolism and preservation. *Rossi's Principles of Transfusion Medicine*. 2022:143-157.
65. Längst E, Crettaz D, Delobel J, et al. In vitro-transfusional model for red-blood-cell study: the advantage of lowering hematocrit. *Blood Transfus*. 2022;21(4):277-288.
66. Huyer G, Liu S, Kelly J, et al. Mechanism of inhibition of protein-tyrosine phosphatases by vanadate and pervanadate. *J Biol Chem*. 1997;272(2):843-851.
67. Gordon JA. Use of vanadate as protein-phosphotyrosine phosphatase inhibitor. *Methods Enzymol*. 1991;201:477-482.
68. Minetti G, Egée S, Mörsdorf D, et al. Red cell investigations: art and artefacts. *Blood Rev*. 2013;27(2):91-101.
69. Willekens FLA, Werre JM, Groenen-Döpp YAM, Roerdinkholder-Stoelwinder B, de Pauw B, Bosman G. Erythrocyte vesiculation: a self-protective mechanism? *Br J Haematol*. 2008;141(4):549-556.
70. Salzer U, Zhu R, Luten M, et al. Vesicles generated during storage of red cells are rich in the lipid raft marker stomatin. *Transfusion*. 2008;48(3):451-462.
71. Prudent M, Crettaz D, Delobel J, Seghatchian J, Tissot JD, Lion N. Differences between calcium-stimulated and storage-induced erythrocytes-derived microvesicles. *Transfus Apher Sci*. 2015;53(2):153-158.
72. Längst E, Tissot JD, Prudent M. Storage of red blood cell concentrates: clinical impact. *Transfus Clin Biol*. 2021;28(4):397-402.
73. Roussel C, Morel A, Dussiot M, et al. Rapid clearance of storage-induced microerythrocytes alters transfusion recovery. *Blood*. 2021;137(17):2285-2298.
74. Safeukui I, Buffet PA, Deplaine G, et al. Quantitative assessment of sensing and sequestration of spherocytic erythrocytes by the human spleen. *Blood*. 2012;120(2):424-430.
75. Bardyn M, Crettaz D, Schmid L, et al. Restoration of physiological levels of uric acid and ascorbic acid reroutes the metabolism of stored red blood cells. *Metabolites*. 2020;10(6):1-18.